# Strength and hydrothermal stability of NiO–stabilized zirconia solid oxide cells fuel electrode supports

Peyman Khajavi, Henrik Lund Frandsen, Laurent Gremillard, Jérôme Chevalier, Peter Vang Hendriksen

# Strength and hydrothermal stability of NiO–stabilized zirconia solid oxide fuel cells electrode supports

Published in the Journal of the European Ceramic Society
https://doi.org/10.1016/j.jeurceramsoc.2021.01.052

Peyman Khajavi[a,*], Henrik Lund Frandsen[a], Laurent Gremillard[b], JérômeChevalier[b], Peter VangHendriksen[a]

[a] Department of Energy Conversion and Storage, Technical University of Denmark, Fysikvej, 2800 Kgs. Lyngby, Denmark
[b] Univ Lyon, INSA-Lyon, CNRS, MATEIS UMR 5510, F-69621 Villeurbanne, France
* Corresponding author: kha@dtu.dk

## Abstract

Long-term, reliable operation of Solid Oxide fuel and electrolysis Cell (SOCs) necessitates cells with high strength and resistance to mechanical degradation. In this work, strength, Young's modulus and Low-Temperature Degradation (LTD) of several zirconia-based SOCs supports are studied. The study shows that replacing 3YSZ with a tetragonal zirconia compound having lower stabilizer contents can improve the strength of porous supports. An enhancement up to 30 % over the-state-of-the-art support (NiO–3YSZ) can be achieved for example with using NiO–2.5YSZ. It is further evidenced that tetragonal zirconia-based SOC components (both Y-doped and Ce-Y co-doped) are susceptible to LTD in the studied range of grain sizes (i.e. ≈ 200−300 nm). Addition of small amount of alumina (0.5 wt%) is observed to increase the LTD resistance of porous supports. The susceptibility to LTD must be considered in designing materials for SOCs, also during materials processing, storage, handling and operation where a dry atmosphere is recommended.

## Keywords

Strength ; Low-temperature degradation ; NiO–Zirconia ; Solid oxide cells ; TTT curve

## 1. Introduction

Despite significant progress in Solid Oxide fuel and electrolysis Cell (SOCs) technologies in recent years, the mechanical properties of such devices still needs to be improved [1-5]. To this end, not only new materials with enhanced mechanical properties are desirable, but also it is essential to investigate the phenomena causing mechanical degradation of the cells.

Anode supported planar SOCs in which the support component is made of a porous Ni(O)–zirconia composite is among the most common cell designs. The support component is an essential part ensuring the mechanical strength of the cells. A strong and degradation resistant support will facilitate long-term, reliable operation and hence further the SOCs technologies. The supports are manufactured using a mixture of NiO and Stabilized Zirconia (SZ), NiO–SZ, and later are reduced to Ni–SZ to be used in SOCs operation. Two common zirconia compounds in this design are 3YSZ (3 mol% $Y_2O_3$ doped zirconia) and 8YSZ (8 mol% $Y_2O_3$ doped zirconia) [6-9]. 3YSZ has a metastable tetragonal crystalline phase. When exposed to external stresses, this tetragonal phase can transform to the monoclinic zirconia, and results in the well-known transformation toughening mechanism as a result of the associated volume expansion [10]. 8YSZ, which has a cubic structure, does not show this toughening mechanism. Both the transformation toughening and a finer grain microstructure typically found for 3YSZ, contribute to enhancing the fracture toughness and strength of NiO–3YSZ SOCs support compared to NiO–8YSZ at room temperature. The transformation toughening effect decreases markedly by increasing temperature. As a result, the fracture toughness of NiO–3YSZ decreases at 800 °C (typical operating temperature of SOCs), yet remains higher than NiO–8YSZ [6,11].

Compared to yttria (Y) doped zirconia, ceria (Ce) doped zirconia ceramics possess a higher fracture toughness and resistance to hydrothermal degradation but a lower strength [12,13]. Ce-Y co-doped ceramics are reported to have optimized fracture toughness, strength and hydrothermal stability [14-16]. Effects of lowering stabilizer content on improving the mechanical properties of stabilized tetragonal zirconia ceramics is well investigated in literature [10,12], but applying this approach for SOCs components and its consequences is not well explored. In our previous work [11], we investigated the fracture toughness of SOCs supports made of six different zirconia compounds: the above-mentioned compounds (3YSZ and 8YSZ) together with four other tetragonal zirconia materials (Y doped and Ce-Y co-doped) having lower stabilizer concertation than 3YSZ. A Ce-Y co-doped material, co-doped with 1.5 mol% $CeO_2$ and 4.5 mol% $YO_{1.5}$ was found to possess the highest fracture toughness, up to 30 % higher compared to the-state-of-the-art (NiO–3YSZ). Furthermore, it was observed that all Ni–tetragonal zirconia based supports (i.e. the reduced supports) were susceptible to hydrothermal degradation, both at low (104 °C) and high temperatures (800 °C).

Low-temperature Degradation (LTD, also sometimes referred to as isothermal aging) of metastable tetragonal zirconia-based ceramics is a well-known phenomenon. It refers to an undesired tetragonal to monoclinic phase transformation during operation that causes severe damage in the ceramic. The aging issue is in particular promoted in humid environments and at temperatures below 400 °C [17-20].

SOCs could be exposed to humidity in several contexts: environment humidity (upon cooling in the sintering step, and during storage and handling of the cells) and moisturized reactants/products (during operation where the steam content can be very high e.g. 90 %, and during thermal cycling where the steam content can typically be controlled). Besides the use in the support component, tetragonal zirconia ceramics are also of interest as the electrolyte material itself in some SOCs designs [21-
24]. Accordingly, hydrothermal degradation of tetragonal zirconia-based components in SOCs (support and electrolyte) may compromise the structural reliability of the devices and its assessment is technologically imperative.

LTD of zirconia-based ceramics is well studied in literature. However, most studies are associated with biomedical applications of the ceramics [25-27]. Works investigating the hydrothermal degradation issue in porous NiO–SZ SOCs supports are still rare. In our previous work [11], we

observed the susceptibility of fuel electrode supports in reduced state to hydrothermal degradation. The LTD was less pronounced in the co-doped samples because of the increased stabilizing effect of $Ce^{3+}$ over $Ce^{4+}$, formed during the reduction of the supports. However, the phenomenon can also be important for the oxidized supports and in electrolytes. Considering the lower LTD susceptibility of Ce-Y co-doped zirconia ceramics, as mentioned earlier, the hydrothermal stability of oxidized zirconia-based supports, with lower stabilizer content than 3YSZ but co-doped with of Ce-Y, should be investigated.

In the present work, the strength and Young's modulus of the NiO–SZ SOCs supports studied in our previous work [11] are investigated to draw a clearer picture of the mechanical properties of the samples. Furthermore, LTD of the NiO–SZ and plain SZ samples at temperatures of 104 and 134 °C is studied and the results are used to develop time-temperature-transformation (TTT) curves for this system.

## 2. Experimental

### 2.1. Materials

Table 1 summarizes characteristics of the NiO–SZ and plain SZ samples studied in this work. The compositions and supplier of the SZ compounds are also provided. The stabilizer(s) content of the zirconia compounds were chosen based on the tetragonal phase stability maps developed in a previous work [28]. The phase stability maps specify the approximate stabilizer concentration to prevent the spontaneous tetragonal to monoclinic phase transformation upon cooling from sintering (which will create microstructural cracks in the ceramic, hence negatively affect its strength), while avoiding overstabilization of the tetragonal phase [28]. The zirconia compounds chosen here are predominantly close to the transformation boundary line for porous materials, whereas one compound (2YSZ, shown in the present work as $3.9YO_{1.5}$-SZ) was chosen to be close to the transformation boundary line for dense ceramics (see ref. [28]).

*Table 1. NiO–Stabilized Zirconia (NiO–SZ) and plain Stabilized Zirconia (plain SZ) samples studied in this work. Compositions and suppliers of the zirconia materials are provided. For example, NiO–14.8$YO_{1.5}$-SZ means a NiO–SZ composite, in which the SZ phase has 14.8 mol% $YO_{1.5}$ as stabilizer (i.e. the SZ phase has the composition of 14.8 mol% $YO_{1.5}$ and 85.2 mol% $ZrO_2$). Microstructure and grain size information of the samples are presented in [11].*

| Sample notation | Stabilizer(s) content of the SZ phase | | Supplier of the SZ material |
|---|---|---|---|
| | $CeO_2$ (mol%) | $YO_{1.5}$ (mol%) | |
| NiO–14.8$YO_{1.5}$-SZ (NiO–8YSZ) | – | 14.8 | Tosoh, Japan |
| NiO–5.8$YO_{1.5}$-SZ (NiO–3YSZ) | – | 5.8 | Tosoh, Japan |
| NiO–5.8$YO_{1.5}$-SZ – 0.5% Alumina | – | 5.8 | Tosoh, Japan |
| NiO–4.9$YO_{1.5}$-SZ (NiO–2.5YSZ) | – | 4.9 | Tosoh, Japan |
| NiO–3.9$YO_{1.5}$-SZ (NiO–2YSZ) | – | 3.9 | Tosoh, Japan |
| NiO–4.6$YO_{1.5}$-SZ | – | 4.6 | Cerpotech, Norway |
| NiO–1.5$CeO_2$ 4.5$YO_{1.5}$-SZ | 1.5 | 4.5 | Nanoe, France |
| NiO–3$CeO_2$ 3.6$YO_{1.5}$-SZ | 3 | 3.6 | Nanoe, France |
| NiO–5$CeO_2$ 3$YO_{1.5}$-SZ | 5 | 3 | Nanoe, France |
| 5.8$YO_{1.5}$-SZ (3YSZ) | – | 5.8 | Tosoh, Japan |
| 4.9$YO_{1.5}$-SZ (2.5YSZ) | – | 4.9 | Tosoh, Japan |
| 1.5$CeO_2$ 4.5$YO_{1.5}$-SZ | 1.5 | 4.5 | Nanoe, France |

The composite (NiO–SZ) and plain (SZ) samples were prepared using tape casting [29,30]. For the composite samples, the typical composition of 55 wt% NiO and 45 wt% SZ was used. From the works on dense zirconia ceramics (mostly on biomedical grade zirconia), alumina is known to improve the LTD resistance of the materials [31-33]. Hence, for one SZ compound, i.e. 3YSZ, NiO–SZ–Alumina composite having 0.5 wt% alumina (in relation to the NiO and SZ content) was also prepared to assess the effect of alumina on the LTD susceptibility. Sintering of the composite samples was done at 1320 °C and 1350 °C. The plain SZ samples were sintered at 1060, 1200 and 1340 °C to obtain samples with different porosities and grain size distribution.

## 2.2. Characterization

The strength of the NiO–SZ samples was measured using four-point bending (with 50 mm between the outer supports, and 25 mm between the loading points), both at room temperature and at 800 °C. The as-sintered tapes were laser cut to rectangular bars with the dimensions of 60 × 6 $mm^2$. The long edges of the samples were polished to remove the microcracks and defects generated during laser cutting to ensure that they do not affect the bending strength. The samples were glued together into a stack with epoxy so that the edges of multiple samples could be polished together. After polishing, the samples were washed repeatedly with acetone in an ultrasonic bath to remove the epoxy [34]. An in-house made rig capable of testing multiple samples was used (for high temperature measurements, the rig enables testing multiple samples in one heat up). Details of the measurement rig can be found elsewhere [35].
The flexural strength (σ) of a rectangular bar in a four-point bending test is given by:

*Equation 1 :* $$\sigma = \frac{3P(L-l)}{2wt^2}$$

where *P* is the load at fracture, *L* is the distance between the outer supports (50 mm), *l* is the distance between the loading points (25 mm), and *W* and *t* are the width and thickness of the specimen, respectively.

Young's modulus of the samples (*E*) was determined from the four-point bending tests using the following equation [34]:

*Equation 2 :* $$E = \frac{3La^2-4a^3}{Wt^3}\frac{\Delta P}{\Delta d}$$

where *ΔP/Δd* is the slope of the load-displacement curve obtained during the measurement, *a* is the distance between the outer support and loading point (12.5 mm), and *L*, *W* and *t* are the parameters introduced in Equation 1.

It is well known that strength of ceramics is dependent on the number, shape, size and distribution of cracks and flaws in their microstructure. This results in a scatter of the strength values of similar samples (having similar composition and preparation) measured under identical conditions. Use of statistical analysis is therefore preferred to evaluate the strength distribution of these brittle materials [36]. In this work, the Weibull statistical analysis was used for strength characterization of the NiO–SZ supports. The strength values measured using Equation 1were sorted in ascending order, and the probability of failure function ($P_f$) was calculated as [37]:

*Equation 3 :* $$P_f = \frac{i-0.5}{N}, i \in \{1,2,\dots,N\}$$

where *N* is the total number of samples.
The two-parameter Weibull distribution model, given as follows, was then used in analyzing the data [36,37]:

*Equation 4 :* $$P_f = 1 - exp\left(-\left(\frac{\sigma}{\sigma_0}\right)^m\right)$$

where *m* and $\sigma_0$ are the Weibull modulus (also called Weibull shape parameter) and Weibull strength (also called Weibull scale parameter), respectively.
For the LTD studies, the plain and composite samples were aged in steam at 104 and 134 °C for different time, ranging from 0.5 to 50 h. The steam pressure at 104 and 134 °C was approximately 0.02 and 0.2 MPa (0.2 and 2 bar), respectively.
The crystalline phase analysis of the as-sintered and aged samples was carried out using X-ray diffraction (XRD) on a Bruker D8 instrument (Bruker, Germany). The method developed by Toraya and co-workers [38] was used to estimate the amounts of monoclinic and tetragonal phases in the samples using the integrated peak intensities of the $(101)_t$, $(111)_m$ and $(\bar{1}11)_m$ planes:

$$\textit{Equation 5}: \quad X_m = \frac{I_m^{(111)} + I_m^{(\bar{1}11)}}{I_m^{(111)} + I_m^{(\bar{1}11)} + I_t^{(101)}}$$

$$\textit{Equation 6}: \quad V_m = \frac{1.311 X_m}{1 + 0.311 X_m}$$

$$\textit{Equation 7}: \quad V_t = 1 - V_m$$

The subscripts *m* and *t* denote the monoclinic and tetragonal phases, respectively.

Microstructural studies were performed using Field Emission Scanning Electron Microscopy (FE-SEM, Carl Zeiss, Germany). The grain size distribution of the samples was evaluated using SEM images of polished and thermally etched samples. Porosity of the samples was determined using their mass and geometrical dimensions.

## 3. Results and discussion

### 3.1. Strength and Young's modulus

#### *3.1.1. NiO–5.8YO1.5-SZ (NiO–3YSZ) benchmark support*

Figure 1 shows the strength of the NiO–5.8$YO_{1.5}$-SZ supports at different porosities measured at room temperature and at 800 °C. The strength values at 13 % porosity reported by Ni and co-workers [34] are also included.

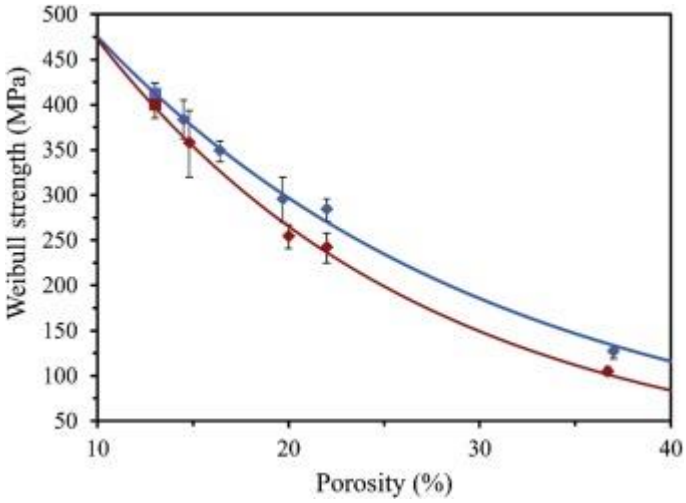


*Figure 1. Weibull strength of NiO–5.8$YO_{1.5}$-SZ as a function of porosity at room temperature (blue markers) and 800 °C (red markers), (♦) measured in this work and (■) in [34]. The fitted exponential curves are shown. (For interpretation of the references to colour in this figure legend, the reader is referred to the web version of this article.).*

The porosity dependency of fracture strength of the NiO–SZ supports can be described by a first order exponential model [9,39,40]:

$$\textit{Equation 8}: \quad \sigma = \tilde{\sigma} exp(-b_\sigma p)$$

where $\tilde{\sigma}$ is the strength of the material at zero porosity, $b_\sigma$ is the porosity dependence constant and *p* is material's porosity. The curves fitted to the room and high temperature strength values (using Eq. 8) are also shown in Figure 1. The $b_\sigma$ values are calculated to be 4.7 (95 % conf. int. of [4.1–5.3]) and 5.8 (95 % conf. int. of [5–6.5]) for room temperature and 800 °C values, respectively. This shows that the decrease in strength by increasing porosity is more pronounced at 800 °C than at room temperature. Ni and co-workers[34] reported the $b_\sigma$ value for similar composite to be 2.6. They used the strength values of oxidized and reduced samples together for fitting, which reduces the accuracy of analysis due to the inherent difference between the mechanical properties of NiO–

5.8$YO_{1.5}$-SZ and Ni–5.8$YO_{1.5}$-SZ composites. Frandsen and co-workers [39] determined the $b_\sigma$ for solid oxide cells' anode supported half cells (having a 10 μm 14.8$YO_{1.5}$-SZ (8YSZ) electrolyte and a 30 μm NiO–14.8$YO_{1.5}$-SZ (NiO–8YSZ) anode, supported on a 300 μm NiO–5.8$YO_{1.5}$-SZ (NiO–3YSZ) support with similar composition as the one used in the current work) to be 8, but they used a smaller range of porosities for the fitting. Deng and co-workers [41] studied the mechanical properties of 5.8$YO_{1.5}$-SZ (3YSZ) ceramics at different porosities. Using the Eq. 8 to fit the strength data reported in [41] the $b_\sigma$ value for plain 3YSZ is calculated to be 4.6. This is close to the room temperature $b_\sigma$ value of the composite material obtained in this work.
Radovic and Lara-Curzio [9] obtained a $b_\sigma$ value of 2.58 (± 0.34) for NiO–14.8$YO_{1.5}$-SZ (NiO–8YSZ, with a cubic zirconia material) composite with a NiO content of ≈ 72 wt%. Although the composition of supports in the current work is different (i.e. 55 wt% NiO) the obtained $b_\sigma$ value indicates that the dependency of strength on porosity is higher in tetragonal zirconia-based supports than for the cubic zirconia ones (as studied in [9]). A similar trend is also observed in the fracture toughness of tetragonal and cubic zirconia based supports [11].

The $\tilde{\sigma}$ values for room temperature and 800 °C are calculated to be 760 and 830 MPa, respectively. These predicted strength values for dense NiO–3YSZ composite are well below the strength of dense 3YSZ (≈ 1020 MPa [42]), which is expected, considering the lower intrinsic mechanical properties of NiO than 3YSZ. Nevertheless, the higher strength of the material at 800 °C than at room temperature may suggest that the model is not suitable for estimating the strength values at porosities below 10 %.
The Young's modulus of NiO–5.8$YO_{1.5}$-SZ samples at different porosities measured at room temperature and 800 °C is presented in Figure 2. The values at room and high temperatures are similar.

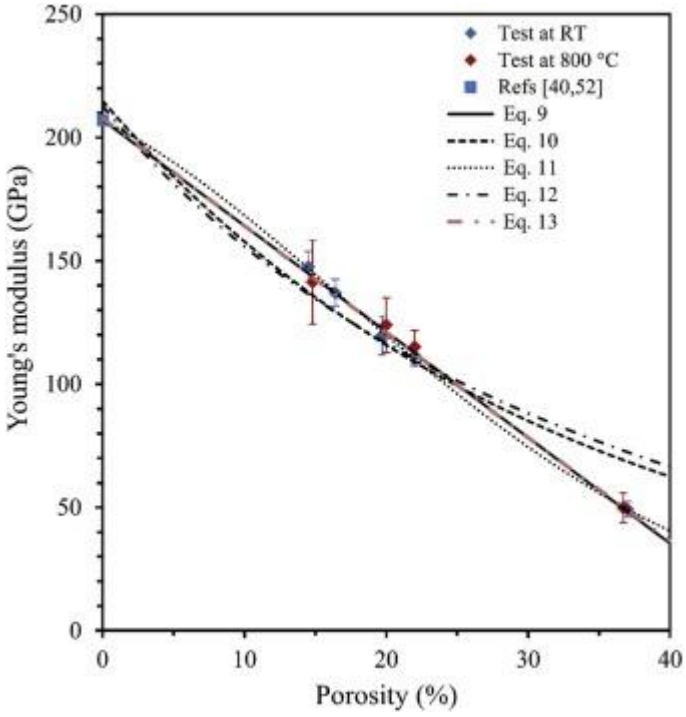


*Figure 2. Young's modulus of NiO–5.8$YO_{1.5}$-SZ as a function of porosity measured at room temperature (blue diamonds) and at 800 °C (red diamonds). The value at zero porosity (blue square) is reported by [40,52]. Different fitted equations to the room temperature Young's modulus data are also shown. (For interpretation of the references to colour in this figure legend, the reader is referred to the web version of this article.).*

The following equations have frequently been used to describe the relation between porosity and Young's modulus of porous ceramics [43,47]:
*Equation 9 :* $E = E_0(1 - b \times p)$

*Equation 10 :* $E = E_0 \cdot e^{-b \times p}$

*Equation 11 :* $E = E_0 \cdot e^{-b \times p + c \times p^2}$

*Equation 12 :* $E = E_0\left(1 + \frac{b \times p}{1-(b+1)\times p}\right)$

*Equation 13 :* $E = E_0(1 - a \times p)^n$

where $E_0$ is Young's modulus at zero porosity, and *a*, *b*, *c* and *n* are empirical constants.
Eqs. 9 and 10 are reported to be applicable to less porous ceramics (< 20 % porosity) [43,48,49], while Eq. 11 can yield better accuracy up to higher porosity levels (≈ 38 %) [46]. Equation 12 gives poor fitting and an unreasonably high $E_0$ when is used to fit experimental data over a wide porosity range [49,50]. Compared to Equation 9 to 12, Equation 13 can be used to describe the Young's modulus-porosity dependency of polycrystalline ceramics over a wider range of porosities; its parameters (*a* and *n*) are correlated to the packing geometry, pore type and structure and grain morphology of the porous ceramic [47,50,51].
Since the Young's modulus values obtained at room temperature and 800 °C were quite consistent, only room temperature data were fitted with above models (Equation 9 to 13). The fitting parameters are presented in Table 2.

*Table 2. Fitting parameters obtained by fitting the Equation 9 to 13 to room temperature Young's modulus-Porosity data of NiO–5.8YO$_{1.5}$-SZ support. The Goodness-of-Fit statistics are given by the Sum of Squares due to Error (SSE), $R^2$, Adjusted $R^2$, and Root Mean Squared Error (RMSE).*

| | Experimental Data | | Experimental dataand assuming $E_0$ = 207 GPa | |
|---|---|---|---|---|
| $E = E_0(1 - b \times p)$ | $E_0$ = 207.3 GPa | *SSE = 17.29* | $E_0$ = 207.1 GPa | *SSE = 17.32* |
| | b = 2.074 | *$R^2$ = 0.9971* | b = 2.073 | *$R^2$ = 0.9987* |
| | | *Adjusted $R^2$ = 0.9961* | | *Adjusted $R^2$ = 0.9984* |
| | | *RMSE = 2.401* | | *RMSE = 2.081* |
| $E = E_0 \cdot e^{-b\times p}$ | $E_0$ = 293.5 GPa | *SSE = 53.06* | $E_0$ = 214.8 GPa | *SSE = 613.1* |
| | b = 4.613 | *$R^2$ = 0.991* | b = 3.086 | *$R^2$ = 0.9537* |
| | | *Adjusted $R^2$ = 0.988* | | *Adjusted $R^2$ = 0.9422* |
| | | *RMSE = 4.206* | | *RMSE = 12.38* |
| $E = E_0 \cdot e^{-b\times p+c\times p^2}$ | $E_0$ = 208.5 GPa | *SSE = 4.826* | $E_0$ = 207 GPa | *SSE = 4.845* |
| | b = 1.456 | *$R^2$ = 0.9992* | b = 1.393 | *$R^2$ = 0.9996* |
| | c = 6.589 | *Adjusted $R^2$ = 0.9984* | c = 6.714 | *Adjusted $R^2$ = 0.9994* |
| | | *RMSE = 1.553* | | *RMSE = 1.271* |
| $E = E_0\left(1 + \frac{b \times p}{1 - (b + 1) \times p}\right)$ | $E_0$ = 452.1 GPa | *SSE = 132.4* | $E_0$ = 212.7 GPa | *SSE = 765.4* |
| | b = -11.72 | *$R^2$ = 0.9775* | b = -3.293 | *$R^2$ = 0.9422* |
| | | *Adjusted $R^2$ = 0.97* | | *Adjusted $R^2$ = 0.9278* |
| | | *RMSE = 6.642* | | *RMSE = 13.83* |
| $E = E_0(1 - a \times p)^n$ | $E_0$ = 228.5 GPa | *SSE = 3.733* | $E_0$ = 207.7 GPa | *SSE = 16.33* |
| | a = 1.68 | *$R^2$ = 0.9994* | a = 2.036 | *$R^2$ = 0.9988* |
| | n = 1.579 | *Adjusted $R^2$ = 0.9987* | n = 1.034 | *Adjusted $R^2$ = 0.9979* |
| | | *RMSE = 1.366* | | *RMSE = 2.333* |

The $E_0$ for a NiO–YSZ system is reported to be ≈ 207 GPa [40,52]. As seen in Table 2, linear (Eq. 9), exponential with quadratic exponent (Eq. 11), and power law (Equation 13) models give the best Goodness of Fit statistics, but $E_0$ is best predicted by Equation 9 and 11. The exponential (Eq. 10) and non-linear (Eq. 12) models yield a poor fitting and an unrealistically high $E_0$.
The fitting was repeated by adding the literature value for Young's modulus at zero porosity (i.e. 207 GPa) to the experimental data obtained in this work, and the results are presented in Table 2 and Figure 2. As seen, the empirical data are described quite well using Eqs. 9,11 and 13, while large disparities among the experimental values and those predicted by Eqs. 10 and 12 are observed. Furthermore, the *n* exponent in Eq. 13 is found to be 1.034, making it very close to a linear function. Selçuk and Atkinson [40] fitted the Eqs. 9,10 and 12 to the Young's modulus of NiO–14.8YO$_{1.5}$-SZ support measured by Impulse Excitation Technique (IET). The authors observed that an accurate fitting in the studied range of porosity (≈ 2–14 %) is possible using all three models. Pihlatie and

co-workers [52] studied the relation between Young's modulus and porosity of NiO–5.8$YO_{1.5}$-SZ support within the porosity range of 10–38 %. The samples had a similar NiO/Zirconia composition as the one applied in the present work, and Young's modulus was measured using IET. The authors reported that the exponential and non-linear fits deviate from experimental values for porosities above 20 % while the linear model gave the best fit over the entire porosity range.
In conclusion, our results show that the porosity dependency of Young's modulus of NiO–SZ supports can be well described with a linear model (Eq. 9) at the studied range of porosities ($p < 35$ %), as also reported in [40,52]. Furthermore, a good consistency between the Young's modulus values obtained by four-point bending (current work) with those measured with IET [52] is observed.

### *3.1.2. NiO–3.9$YO_{1.5}$-SZ (NiO–2YSZ) support*

The as-sintered NiO–3.9$YO_{1.5}$-SZ support contained several macrocracks and were fractured into smaller pieces. From the XRD analysis, it was found that the zirconia phase in the as-sintered sample contained 93 % of monoclinic phase. In addition, SEM images of the sample (Figure 3) showed extensive number of microcracks and defects.

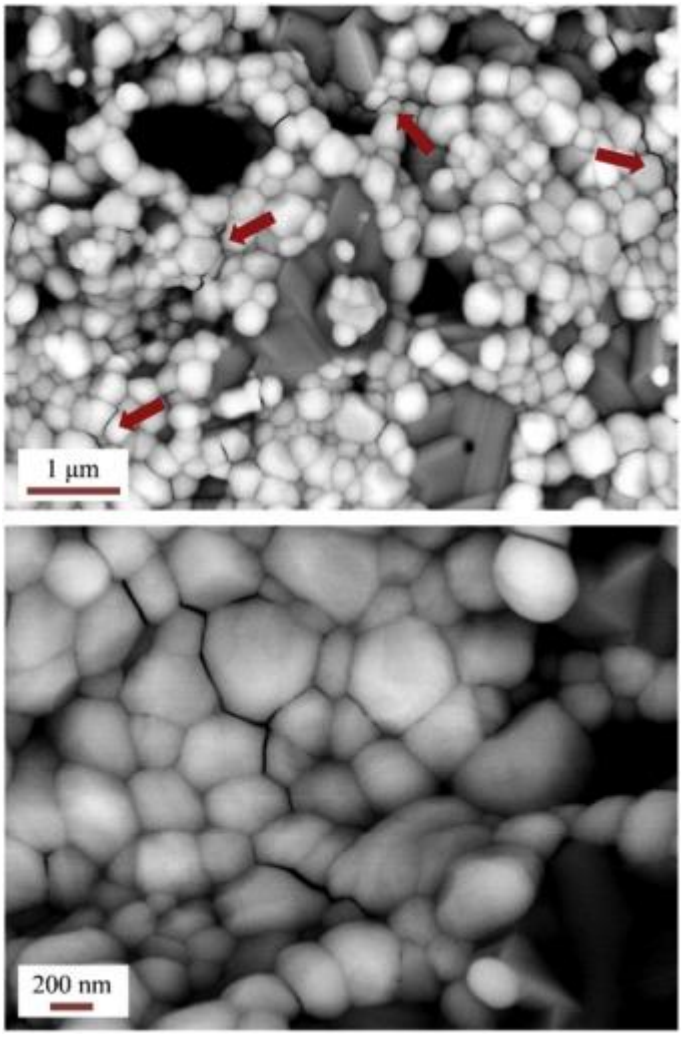


*Figure 3. SEM micrographs of as-sintered NiO–3.9$YO_{1.5}$-SZ support. The small (white) and large (gray) grains are zirconia and NiO, respectively. The arrows show the cracks generated most likely due to the tetragonal to monoclinic phase transformation upon cooling.*

The tetragonal to monoclinic (t-m) phase transformation is characterized by a 3–5% volume expansion. If this transformation occurs to a large extent upon cooling from the sintering temperature, numerous cracks will be generated in the ceramic [12]. Considering the high amount of monoclinic phase in the as-sintered NiO–3.9$YO_{1.5}$-SZ sample (93 %), the formation of these macro- and micro- cracks can thus be ascribed to the t-m transformation upon cooling.

The studies on the stability of the tetragonal phase in doped zirconia compounds in our previous work [28] showed that the 2 mol% $Y_2O_3$ doped zirconia will contain a large amount of monoclinic phase (74.4 %) when calcined in the powder form at 1350 °C. On the other hand, in a sintered ceramic state (with a density of 98 % of the theoretical density) the tetragonal phase was fully retained (see Table 3 of [28]). The NiO–3.9$YO_{1.5}$-SZ support prepared in this work had a rather high porosity (≈ 25 %). In addition, it is reported that the presence of NiO in a NiO–SZ composite facilitate the tetragonal to monoclinic phase transformation [11]. The high porosity of the NiO–3.9$YO_{1.5}$-SZ support and the presence of NiO thus explain the here observed large amount of monoclinic phase in the sample.

*Table 3. Weibull strength, Weibull modulus and Young's modulus of NiO–SZ samples at room temperature and 800 °C. For each modality ≈ 10 specimens were tested. This low number of measurements makes obtaining precise Weibull modulus difficult.*

| Material | Porosity (%) | Tested at RT | | | Tested at 800 °C | | |
|---|---|---|---|---|---|---|---|
| | | $\sigma_0$ (MPa)‡ | $m$‡ | $E$ (GPa)* | $\sigma_0$ (MPa)‡ | $m$‡ | $E$ (GPa)* |
| NiO–14.8$YO_{1.5}$-SZ | 7.5 | 190 (173−207) | 5.3 (3.4−8.1) | 156 (6.7) | 200 (167−233) | 3.8 (2.2−7) | 154.4 (2.6) |
| NiO–4.6$YO_{1.5}$-SZ | 31 | 161 (157−173) | 11.4 (6.9−19.2) | 68.9 (3.2) | – | – | – |
| | 35 | 147 (138−156) | 8.9 (5.4−15) | 55.8 (1.5) | 110 (95−126) | 4.4 (2.6−8) | 49.6 (7.1) |
| NiO–4.9$YO_{1.5}$-SZ | 18.5 | 414 (395−431) | 12.9 (7.9-21.6) | 139.7 (4.5) | 382 (338-426) | 4.7 (2.9-7.9) | 144.7 (7.8) |
| NiO–1.5$CeO_2$ 4.5$YO_{1.5}$-SZ | 20.5 | 311 (295−326) | 11.8 (7−20.6) | 112.7 (2.8) | 321 (303−337) | 11.9 (6.9−21.8) | 132.6 (5.6) |
| NiO–3$CeO_2$ 3.6$YO_{1.5}$-SZ | 23.5 | 309 (298−318) | 18.4 (10.9−32.2) | 104.7 (4.1) | 249 (227−269) | 7 (4.2−12.5) | 118.7 (3.9) |
| NiO–5$CeO_2$ 3$YO_{1.5}$-SZ | 23.5 | 265 (240−289) | 6.3 (3.7−11) | 101.4 (1.9) | – | – | – |
| | 25 | 231 (213−248) | 7.3 (4.4−12.3) | 84.5 (4.8) | – | – | – |

‡ Numbers in parentheses show the 90 % confidence intervals.
* Numbers in parentheses show the standard deviation.

### *3.1.3. Other zirconia-based SOCs supports*

The measured fracture strength and Young's modulus of the new tetragonal zirconia-based support materials together with the porosity of the samples are given in Table 3. Also, the fracture strength of NiO–14.8$YO_{1.5}$-SZ, having the cubic structure, is listed. It is observed to be significantly lower than the samples with the tetragonal phase. The same trend was observed for the fracture toughness of these samples [11] and was explained as an effect of transformation toughening and finer grained microstructure of the tetragonal zirconia based supports. Weibull plots showing the strength distribution for the different samples are shown in Figure 4.

Since the samples were at different porosities, in order to compare their strength with that of the state-of-the-art NiO–5.8$YO_{1.5}$-SZ support, the above fitted strength-porosity models were used (Figure 1); the strength values of NiO–5.8$YO_{1.5}$-SZ were estimated at the corresponding porosities for each of the measurements to make a porosity corrected benchmark for the measured strengths.

Figure 5 shows the Weibull strength of the supports with different stabilized zirconia compounds and the strength values for the NiO–5.8$YO_{1.5}$-SZ at the corresponding porosities (estimated using the developed strength-porosity models).

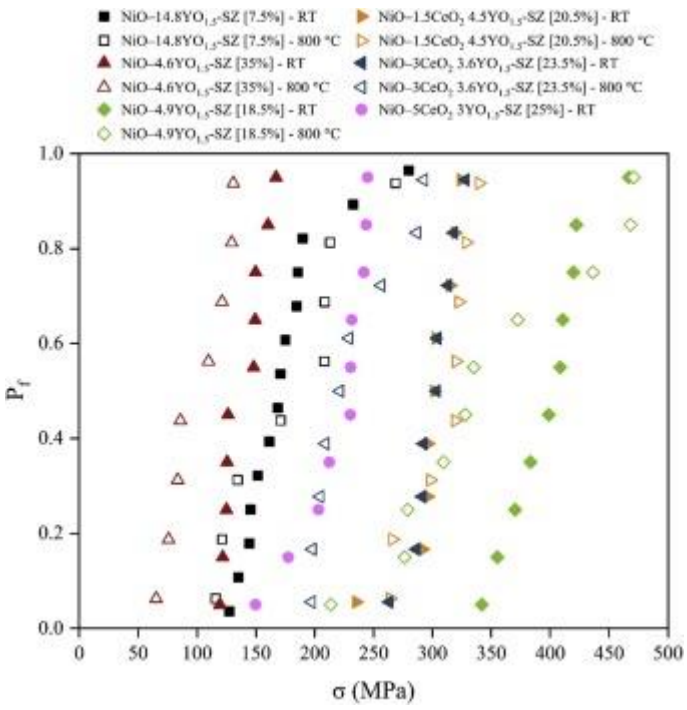


*Figure 4. Weibull plots showing the strength distribution of samples tested at room temperature and at 800 °C. The porosity of the samples is shown in the brackets.*

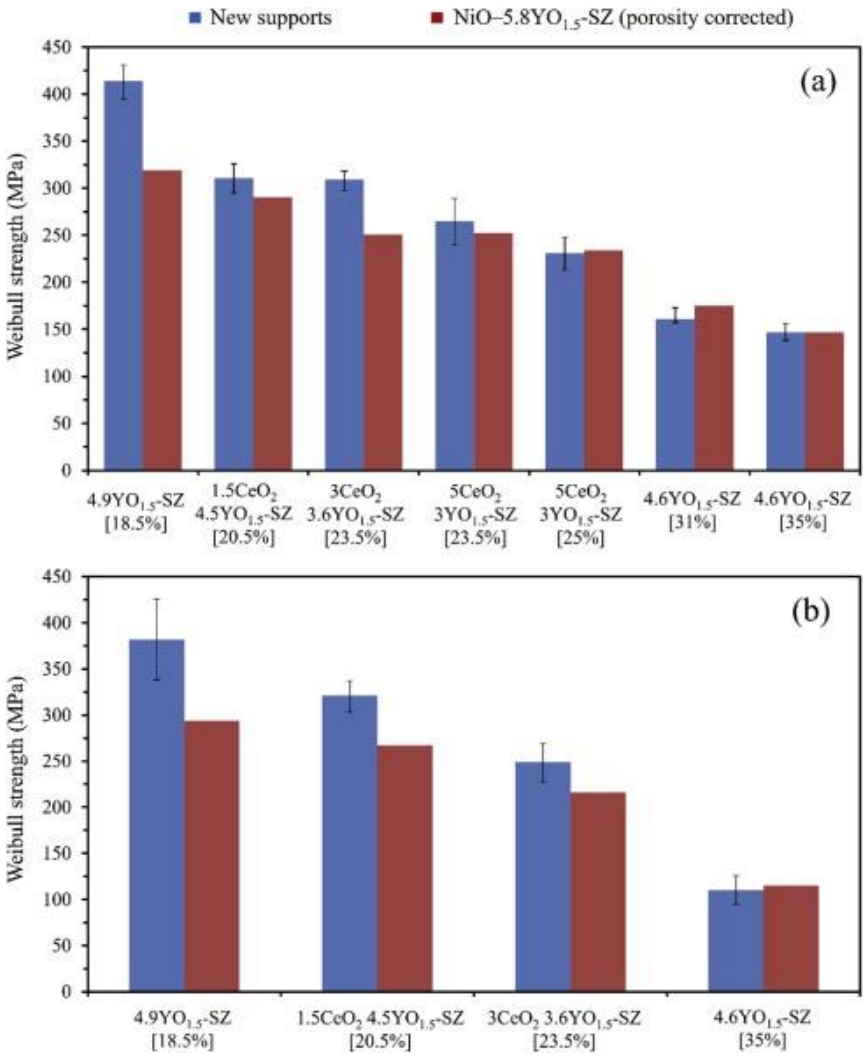


*Figure 5. Weibull strength of the different NiO–tetragonal zirconia supports (blue bars) compared to the estimated value for NiO–5.8YO1.5-SZ substrate at the corresponding porosities, at (a) room temperature and (b) 800 °C. The porosity of the samples is shown in the brackets. The error bars show the 90 % confidence intervals.*

The NiO–4.9$YO_{1.5}$-SZ exhibits a significantly higher strength (≈ +30 %) both at room temperature and 800 °C. In addition, the 1.5$CeO_2$ 4.5$YO_{1.5}$-SZ and 3$CeO_2$ 3.6$YO_{1.5}$-SZ based supports also show an improved strength over the state-of-the-art. The strength values in other compounds are relatively comparable.

The average grain sizes of the zirconia phase in 4.9$YO_{1.5}$-SZ, 1.5$CeO_2$ 4.5$YO_{1.5}$-SZ and 3$CeO_2$ 3.6$YO_{1.5}$-SZ based supports are 288, 283, and 313 nm, respectively, relatively larger than that of 5.8$YO_{1.5}$-SZ based support (i.e. 226) (see Table 4). The observed improved strength in the samples, despite having a larger grain size than the 5.8$YO_{1.5}$-SZ, can be explained by the higher transformability of their zirconia compounds, due to their lower stabilizer content. This is in line with the Raman spectroscopy analysis of the NiO–5.8$YO_{1.5}$-SZ and NiO–4.9$YO_{1.5}$-SZ supports carried out in our previous work [11], where we found larger amounts of monoclinic phase on the fractured surfaces of NiO–4.9$YO_{1.5}$-SZ.

*Table 4. The samples investigated in the LTD experiments, their average grain sizes and the porosity of each individual piece of sample tested for LTD. The uncertainty of the measured porosities is about 1-2%. The numbers in parentheses show the standard deviation.*

| Sample notation | Porosity (%) | Grain size (nm) |
|---|---|---|
| NiO–5.8$YO_{1.5}$-SZ | 20 | 226 (94) |
| NiO–5.8$YO_{1.5}$-SZ – 0.5% Alumina | 12.5 | 249 (92) |
| | 21 | 228 (94) |
| NiO–4.9$YO_{1.5}$-SZ | 18.5 | 288 (117) |
| NiO–1.5$CeO_2$ 4.5$YO_{1.5}$-SZ | 15.5 | 283 (138) |
| | 21 | 230 (81) |
| NiO–3$CeO_2$ 3.6$YO_{1.5}$-SZ | 25.5 | 313 (131) |
| NiO–5$CeO_2$ 3$YO_{1.5}$-SZ | 23.5 | 327 (128) |
| 5.8$YO_{1.5}$-SZ | 45.5 | 40 (10) |
| | 25 | 149 (34) |
| | 4.5 | 238 (84) |
| 4.9$YO_{1.5}$-SZ | 42.5 | – |
| | 21 | 132 (25) |
| | 1.5 | 188 (77) |
| 1.5$CeO_2$ 4.5$YO_{1.5}$-SZ | 34 | – |
| | 10.5 | 156 (35) |
| | 6.5 | 275 (135) |

The XRD analysis of different tetragonal zirconia based supports after aging for 850 h at 800 °C (high-temperature degradation (HTD), see Figure 7 of [11]) indicated the vulnerability of Ni–4.9$YO_{1.5}$-SZ support to HTD: a large amount of monoclinic phase (≈ 35 %) was observed after the HTD experiment. Therefore, despite the significantly high strength of the NiO–4.9$YO_{1.5}$-SZ support, as observed in the present study, with its current grain size range (i.e. average of 288 nm), it cannot be a reliable support component for use in SOCs, as it is not stable for long-term operation. The 1.5$CeO_2$ 4.5$YO_{1.5}$-SZ based support shows superior HTD resistance and fracture toughness, resulting from an enhanced stabilizing effect of $Ce^{3+}$ formed during reduction [11]. This together with the higher strength of this support compared to the-state-of-the-art material (Figure 5) may suggest it as an alternative for the SOCs fuel electrode support component, providing enhanced strength, toughness and resistance to high-temperature degradation. In addition, the LTD resistance of the samples in their oxidized form should be assessed, as this also affects the suitability of the materials for the application. This has been addressed in the following sections.

### 3.2. LTD results

Table 4 presents the samples studied in the LTD experiments. The porosity and grain sizes of the specific samples are also provided.

#### *3.2.1. NiO–SZ samples*

Figure 6 shows the amount of monoclinic phase formed on aging of the NiO–5.8$YO_{1.5}$-SZ samples, with and without alumina and at different grain sizes. It is observed that:

• For the samples containing alumina (i.e. red and green curves) aged at 134 °C, it is seen that the sample with smaller average grain size and higher porosity (green curve) is stable after 50 h of aging (no monoclinic phase is detected), which is not the case for the larger grained and less porous sample.

• Considering the samples having similar average grain size and porosity, but with and without alumina (i.e. the blue and green curves) aged at 134 °C, it is observed that the sample without alumina is very sensitive to aging, while no monoclinic phase is formed in the alumina containing sample.

• The crystalline phase analysis of the samples aged at 104 °C for 20 h showed no monoclinic zirconia in the samples with average grain size of 226 and 228 nm, whereas minor amount of monoclinic phase (≈ 5.5 %) was detected in the sample with the average grain size of 249 nm and 12.5 % porosity.

Accordingly, it is concluded that presence of alumina significantly increases the LTD resistance of the NiO–SZ composites. The improved LTD resistance of dense zirconia ceramics (without NiO) having a small amount of alumina was already reported in literature (as mentioned earlier in the experimental section). The beneficial effect of small amounts of alumina is verified here, for a porous zirconia-containing composite.

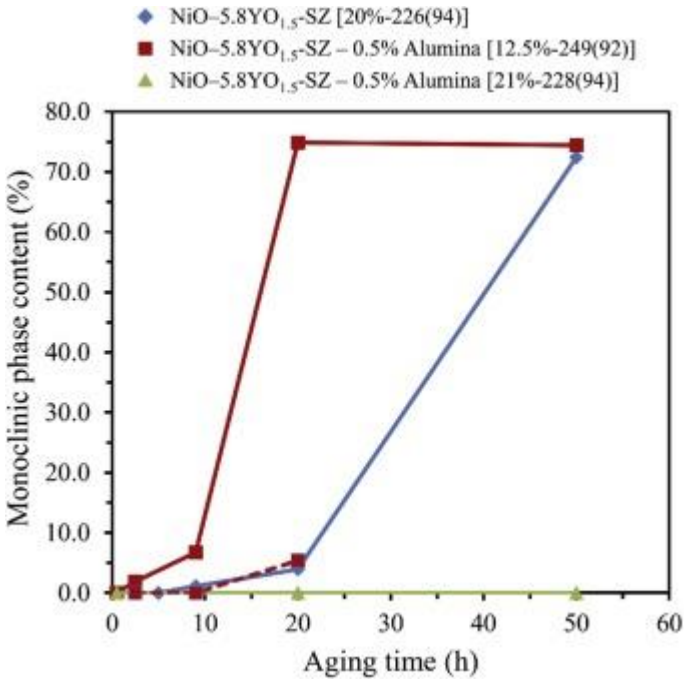


*Figure 6. Monoclinic content of NiO–5.8$YO_{1.5}$-SZ supports (with and without alumina and at different grain sizes) as a function of aging time at 134 °C (solid lines) and 104 °C (dashed lines). Porosity and average grain size of the samples are shown in brackets. The numbers in parentheses represent the standard deviation from the average grain size.*

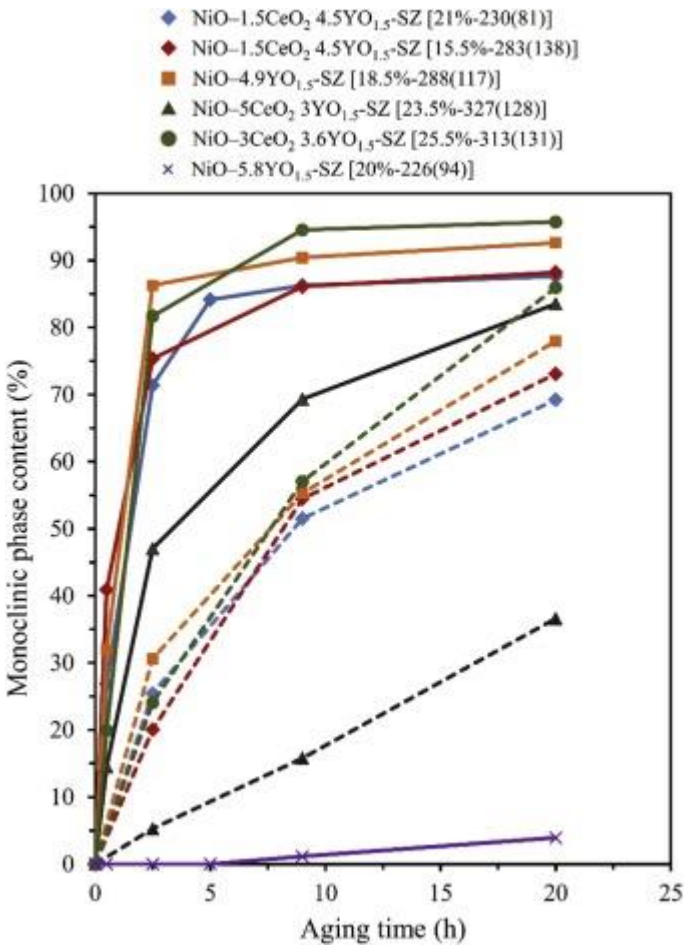


*Figure 7. Monoclinic content of NiO–SZ supports as a function of aging time at 134 °C (solid lines) and 104 °C (dashed lines). Porosity and average grain size of the samples are shown in brackets. The numbers in parentheses represent the standard deviation from the average grain size.*

For the alumina containing samples, the observed lower stability of the tetragonal phase in the sample with larger average grain size and lower porosity could be a consequence of both grain size and porosity. As seen inFigure 6, after 10 h of aging at 134 °C, the tetragonal phase in NiO–5.8$YO_{1.5}$-SZ – 0.5 % Alumina [21 %-228(94)] is completely stable, while 6.7 % of the monoclinic phase is detected in NiO–5.8$YO_{1.5}$-SZ – 0.5 % Alumina [12.5 %-249(92)]. This might be due to the larger grain size of the latter. A further aging from 9 to 20 h causes a substantial phase transformation in this sample. A possible explanation for this pronounced degradation is the relatively low porosity of the sample: a lower porosity means that larger part of the internal stresses arising due to the tetragonal to monoclinic phase transformation that has occurred earlier is exerted on neighboring tetragonal grains, promoting the hydrothermal degradation of the grains [53]. A more porous structure can accommodate a larger part of the aforementioned stresses, thus reducing the driving force for the phase transformation in non-transformed tetragonal grains, as observed in NiO–5.8$YO_{1.5}$-SZ – 0.5 % Alumina [21 %-228(94)].

The monoclinic phase content of NiO–4.9$YO_{1.5}$-SZ, NiO–1.5$CeO_2$ 4.5$YO_{1.5}$-SZ, NiO–3$CeO_2$ 3.6$YO_{1.5}$-SZ and NiO–5$CeO_2$ 3$YO_{1.5}$-SZ after aging are presented inFigure 7. For comparison, the aging result of NiO–5.8$YO_{1.5}$-SZ sample (without alumina) is also included.

The NiO–5$CeO_2$ 3$YO_{1.5}$-SZ has the highest aging stability compared to the other three compositions, which can be attributed to its relatively larger stabilizer content, and also the higher amount of doped ceria (Ce doped zirconia ceramics, typically, have higher aging resistivity as discussed earlier). The aging results of NiO–1.5$CeO_2$ 4.5$YO_{1.5}$-SZ samples having two different grain sizes and porosities show the high susceptibility of the samples to LTD. The lower stability of the new compounds can also be observed in the large amount of phase transformation after aging at 104 °C.

The results show that NiO–SZ supports with a tetragonal stabilized zirconia compound are sensitive to LTD at the studied temperatures. The LTD susceptibility of the new supports is markedly higher than the NiO–5.8$YO_{1.5}$-SZ. This can be explained by the lower content of stabilizer in their zirconia

phase. Here, an important point to consider is that LTD of zirconia ceramics typically has a maximum rate at temperatures between 250−400 °C [20,54,55]. Therefore, technologically an estimation of LTD rate of the samples is necessary at this range of temperatures. This is partly covered later in Section 3.2.3. using the constructed Time-Temperature-Transformation (TTT) curves.

### *3.2.2. Plain SZ samples (without NiO)*

The plain SZ samples sintered at 1060 °C were highly porous (i.e. 34–46 %). No monoclinic phase was found in the samples after aging at 134 °C for a duration as long as 50 h. This can be explained by the ultrafine microstructure of the samples due to the low sintering temperature. For example, the average grain size of the $5.8YO_{1.5}$-SZ sample was found to be 40 nm.
Figure 8 shows the amount of monoclinic phase found in the $5.8YO_{1.5}$-SZ, $4.9YO_{1.5}$-SZ, and $1.5CeO_2$ $4.5YO_{1.5}$-SZ samples sintered at 1200 °C after aging. The $5.8YO_{1.5}$-SZ was completely stable even after 50 h of aging, while a significant amount of monoclinic phase is formed in $4.9YO_{1.5}$-SZ and $1.5CeO_2$ $4.5YO_{1.5}$-SZ. The $4.9YO_{1.5}$-SZ was the least stable at these aging conditions. Minor amount of monoclinic phase (i.e. < 1.5 %) was observed in $4.9YO_{1.5}$-SZ and $1.5CeO_2$ $4.5YO_{1.5}$-SZ after 20 h aging at 104 °C (not shown in Figure 8).

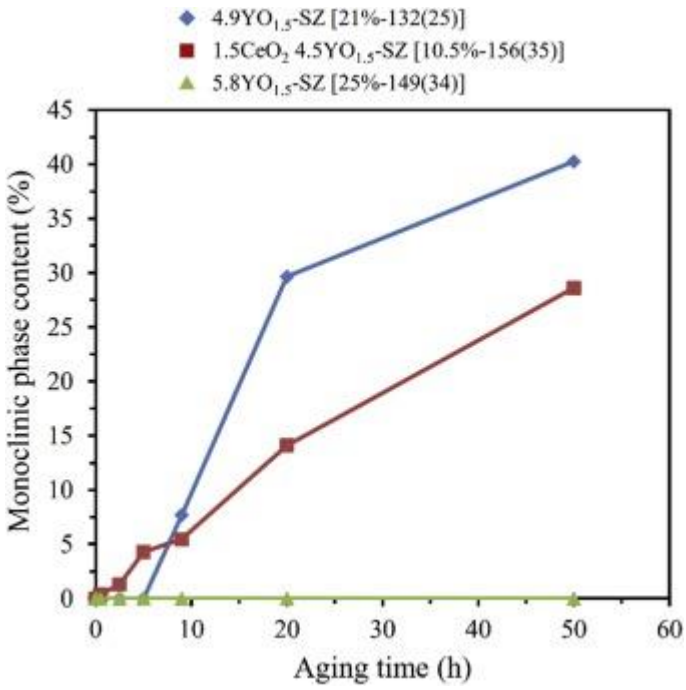


*Figure 8. Monoclinic content of plain SZ samples sintered at 1200 °C as a function of aging time at 134 °C. Porosity and average grain size of the samples are shown in brackets. The numbers in parentheses represent the standard deviation from the average grain size.*

The aging results of the plain SZ samples sintered at 1340 °C (Figure 9) showed a dramatically increased aging susceptibility as a consequence of having larger average grain sizes. $4.9YO_{1.5}$-SZ had the highest sensitivity to LTD (despite having smaller grain size).

The solid electrolyte in a SOC is a dense component. As an example, a 3YSZ electrolyte can have an average grain size of ≈ 300−500 nm [56,57]. The plain $5.8YO_{1.5}$-SZ (3YSZ) sintered at 1340 °C studied in this work has smaller grain size and lower density, that both would decrease its susceptibility to LTD compared to a typical 3YSZ electrolyte. Hence, the observed aging sensitivity of the plain zirconia samples well represent the importance of taking the LTD of tetragonal zirconia-based SOCs electrolytes into account.
Furthermore, comparing the aging results of plain and composite samples, it can be concluded that NiO does not have a significant effect on the aging susceptibility of the tetragonal zirconia in NiO–SZ composites.

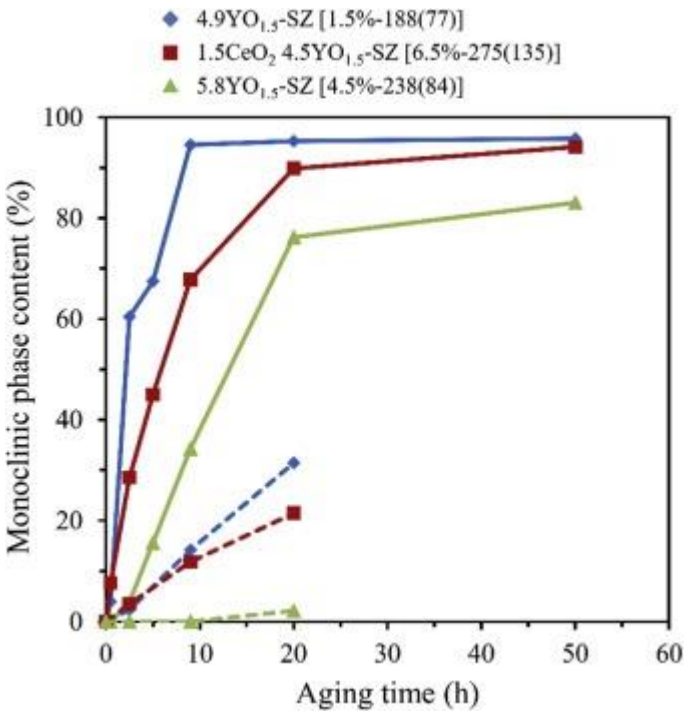


*Figure 9. Monoclinic content of plain SZ samples sintered at 1340 °C as a function of aging time at 134 °C (solid lines) and 104 °C (dashed lines). Porosity and average grain size of the samples are shown in brackets. The numbers in parentheses represent the standard deviation from the average grain size.*

It has been reported that the LTD in zirconia compounds can be promoted in the presence of mechanical stresses [58]. A SOC is typically made of different components, including fuel and oxygen electrodes and electrolyte. The mismatch among the thermal expansion coefficients of the cell components causes residual stresses to form during cooling from the sintering step, during operation and thermal cycling [59,60]. Such stresses would likely accelerate the isothermal degradation of the tetragonal zirconia components, so it becomes larger than what is reported in this work (considering only one component).

### *3.2.3. Time-temperature-transformation (TTT) curves*

Using the aging results of the composite and plain zirconia samples obtained, time-temperature-transformation (TTT) curves, that map the time required for evolution of a certain amount of monoclinic phase at different temperatures, can be developed. For instance, Figure 10 a,b shows the 10 % monoclinic lines for NiO–SZ and plain SZ samples. The TTT diagrams have not previously been developed for NiO–SZ supports, although they can be used to rationalize the kinetics of LTD in these systems.

The aging temperatures applied in this work (i.e. 104 and 134 °C) provide the TTT curves for a narrow range of temperatures (Figure 10) only. For zirconia ceramics, it is known that the TTT curves typically have a C-shape, with a "nose" temperature, i.e. the temperature at which the tetragonal to monoclinic phase transformation occurs with a maximum rate, which is typically found to be between 250−400 °C (as also discussed earlier) [20,54,55]. Extrapolating the TTT curves developed in this work to such temperatures, it is estimated that the 10 % monoclinic phase formation occurs with a very high rate, i.e. in ≈ 10−100 s for the new stabilized zirconia compounds and in ≈ 1000s for the $5.8YO_{1.5}$-SZ based substrate. This extrapolation is rough, because it is based on a limited amount of data and because TTT curves do not follow exactly a linear variation of temperature-time up to the nose temperature, so the generated curves are illustrative and have high uncertainty. Nevertheless, they indicate that technologically (e.g. during cooling of a SOC stack) it is crucial to take into account the risk of LTD at low and moderate temperatures.

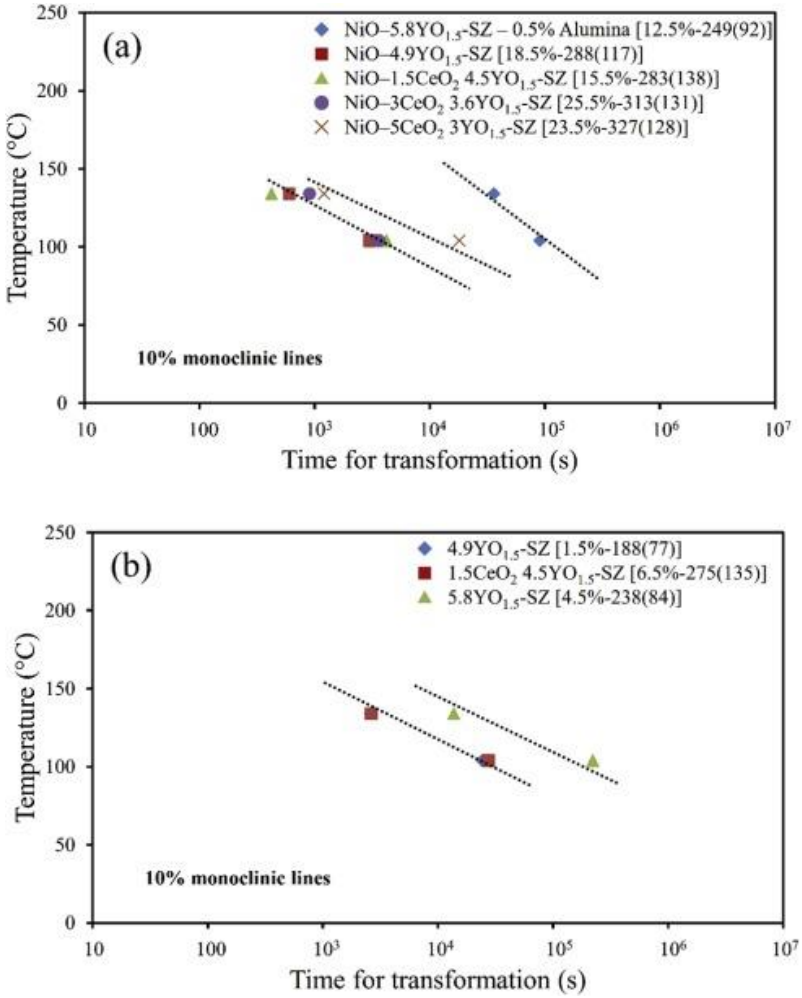


*Figure 10. Time-temperature-transformation (TTT) curves of (a) NiO–SZ and plain SZ samples with different stabilizer composition.*

LTD in SOCs components creates challenges for different reasons. The volume expansion associated with the tetragonal to monoclinic phase transformation (occurring during LTD) generates cracks in the microstructure. This can negatively affect the strength of tetragonal zirconia ceramics. The drop in the bulk strength is dependent on the extent of transformation and thickness of the degraded layer [61,62]. For example, Marro and co-workers [61] reported on approximately 6 and 13 % decrease in the strength of 3Y-TZP ceramics after aging experiments that had resulted in 3 and 10 μm thick degraded layers, respectively. As observed in this work, the extent of phase transformation caused by LTD is lower in components with higher porosities. Nonetheless, compared to dense ceramics, in a porous structure (like SOCs supports) the exposure to humidity would be easier throughout the material. Hence, the LTD-formed cracks would be created in the entire ceramic, and a more severe effect of LTD on the strength is expected. This explains why the SOC supports studied in this work lost their structural integrity after aging experiments, such that they crumbled upon subsequent handling.

Another challenge is the mechanical degradation caused by slow crack growth (SCG), which is accelerated in the presence of LTD-formed cracks as the SOCs are exposed to moisturized atmosphere. The threshold intensity factor ($K_{I0}$) in zirconia ceramics at different porosities is approximately 56 % of the fracture toughness [63]. In other words, the cracks can propagate at the stress level approximately half that of the stress for fast fracture, regardless of the porosity of the ceramic (hence it will be an issue in both porous support and dense electrolyte). An additional challenge is that micrometric cracks and defects formed by LTD in thin (typically < 50 μm) SOCs electrolytes can cause unwanted leakages and, hence, contact of reactants normally separated by the electrolyte in SOCs (proper performance of SOCs requires a fully dense electrolyte). This negatively affects the electrochemical performance and even causes failure of the cells. In addition, LTD-formed cracks can compromise the strength of the electrolyte due to the low thickness of this component.

Generally, the results of this study show that by increasing the transformability of tetragonal zirconia, the strength of porous supports increases, while it also increases the LTD in the oxidized supports. As discussed in our previous work [11], having ceria as a co-dopant can minimize the extent of hydrothermal degradation in the reduced form, but the LTD issue remains problematic in the oxidized supports even in the Ce-Y co-doped samples, as concluded here.
The LTD studies on the NiO–SZ and plain SZ samples show that tetragonal zirconia-based SOCs components (support and electrolyte) are highly vulnerable to LTD even at the small grain sizes studied here (i.e. below 300 nm). Although the variation in the strength of samples with aging time and temperature was not investigated in this work, our findings indicate that to ensure the structural integrity of SOCs the LTD issue needs to be carefully considered in materials selection and cell operation. Possible alternatives should be considered to increase the LTD resistance of SOCs components, such as by developing ceramic processing routes to obtain finer grained microstructures, with grain sizes well below 200 nm. In addition, this phenomenon points to the necessity of ensuring a dry atmosphere in SOC stacks through thermal cycling (irrespective of the stabilizers content of stabilized zirconia compound) and under storage.

## 4. Conclusions

In this work, strength and Young's modulus of porous NiO–SZ SOCs fuel electrode supports were studied. The dependence of both strength and Young's modulus on porosity was studied in detail. The LTD susceptibility of NiO–SZ and plain SZ (without NiO) samples was also investigated. The results of the study can be summarized as follows:

- NiO–4.9$YO_{1.5}$-SZ had the highest strength. Compared to the state-of-the-art NiO–5.8$YO_{1.5}$-SZ support it showed approximately 30 % strength improvement. Among the Ce-Y co-doped zirconia compounds, the NiO–1.5$CeO_2$ 4.5$YO_{1.5}$-SZ and NiO–3$CeO_2$ 3.6$YO_{1.5}$-SZ showed improved strength by as much as 23 % in comparison to the NiO–5.8$YO_{1.5}$-SZ support.
- The aging studies of NiO–SZ and plain SZ samples showed that tetragonal zirconia-based SOCs components (in the studied range of grain sizes, i.e. ≈ 200–300 nm) are highly sensitive to LTD. Decreasing the stabilizer content of the zirconia phase (from 5.8 mol% $YO_{1.5}$) increased the LTD susceptibility, even in the Ce-Y co-doped samples.
- Approximated TTT curves of NiO–SZ supports predicted a very high rate of transformation (in the order of minutes) in steam at temperatures around 300 °C. Therefore, to avoid the tetragonal to monoclinic phase transformation in tetragonal zirconia-based SOCs components (irrespective of the stabilizer content of the zirconia material) it is important to use dry atmosphere upon cooling in sintering of ceramics, through thermal cycling of cells/stacks, and also during the storage of the materials.
- Alumina was confirmed to act as LTD inhibitor in porous NiO–SZ composite, similar to the known trend in dense zirconia ceramics. Addition of 0.5 wt% alumina improved the LTD resistance of the support.
- The LTD results of plain and composite samples revealed no clear effect of NiO on the aging of the zirconia phase in NiO–SZ composites.
- The Young's modulus of NiO–5.8$YO_{1.5}$-SZ supports in the porosity range of 0–35 % was concluded to be a linear function of porosity.

## Declaration of Competing Interest

The authors report no declarations of interest.

## Acknowledgements

The authors would like to thank Innovation Fund, Denmark for the financial support of this study under the framework of SYNFUEL (sustainable synthetic fuels from biomass gasification and electrolysis) project (File No. 4106-00006B).

## References


1. A. Nakajo, Z. Wuillemin, J. Van herle, D. Favrat, **Simulation of thermal stresses in anode-supported solid oxide fuel cell stacks. Part I: probability of failure of the cells,** J. Power Sources, 193 (2009), pp. 203-215
2. A. Nakajo, J. Kuebler, A. Faes, U.F. Vogt, H.J. Schindler, L.K. Chiang, S. Modena, J. Van Herle, T. Hocker, **Compilation of mechanical properties for the structural analysis of solid oxide fuel cell stacks. Constitutive materials of anode-supported cells,** Ceram. Int., 38 (2012), pp. 3907-3927
3. T. Klemensø, D. Boccaccini, K. Brodersen, H.L. Frandsen, P.V. Hendriksen, **Development of a novel ceramic support layer for planar solid oxide cells,** Fuel Cells, 14 (2014), pp. 153-161
4. B. Charlas, D.W. Ni, H.L. Frandsen, K. Brodersen, M. Chen, **Mechanical properties of supports and half-cells for solid oxide electrolysis influenced by alumina-zirconia composites,** Fuel Cells, 17 (2017), pp. 132-143
5. H.L. Frandsen, M. Makowska, F. Greco, C. Chatzichristodoulou, D.W. Ni, D.J. Curran, M. Strobl, L.T. Kuhn, P.V. Hendriksen, **Accelerated creep in solid oxide fuel cell anode supports during reduction,** J. Power Sources, 323 (2016), pp. 78-89
6. G. Pećanac, J. Wei, J. Malzbender, **Fracture toughness of solid oxide fuel cell anode substrates determined by a double-torsion technique,** J. Power Sources, 327 (2016), pp. 629-637
7. J. Wei, T. Osipova, J. Malzbender, M. Krüger, **Mechanical characterization of SOFC/SOEC cells,** Ceram. Int., 44 (2018), pp. 11094-11100
8. S. Goutianos, H.L. Frandsen, B.F. Sørensen, **Fracture properties of nickel-based anodes for solid oxide fuel cells,** J. Eur. Ceram. Soc., 30 (2010), pp. 3173-3179
9. M. Radovic, E. Lara-Curzio, **Mechanical properties of tape cast nickel-based anode materials for solid oxide fuel cells before and after reduction in hydrogen,** Acta Mater., 52 (2004), pp. 5747-5756
10. R.H.J. Hannink, P.M. Kelly, B.C. Muddle, **Transformation toughening in zirconia-containing ceramics,** J. Am. Ceram. Soc., 83 (2000), pp. 461-487
11. P. Khajavi, P.V. Hendriksen, J. Chevalier, L. Gremillard, H.L. Frandsen, **Improving the fracture toughness of stabilized zirconia-based solid oxide cells fuel electrode supports: effects of type and concentration of stabilizer(s),** J. Eur. Ceram. Soc., 40 (2020), pp. 5670-5682
12. I. Nettleship, R. Stevens, **Tetragonal zirconia polycrystal (TZP) - a review,** Int. J. High Technol. Ceram., 3 (1987), pp. 1-32
13. J. Chevalier, L. Gremillard, **Ceramics for medical applications: a picture for the next 20 years,** J. Eur. Ceram. Soc., 29 (2009), pp. 1245-1255
14. J.-D. Lin, J.-G. Duh, **Fracture toughness and hardness of ceria-and yttria-doped tetragonal zirconia ceramics,** Mater. Chem. Phys., 78 (2002), pp. 253-261
15. J.D. Lin, J.G. Duh, **Correlation of mechanical properties and composition in tetragonal CeO2-Y2O3-ZrO2 ceramic system,** Mater. Chem. Phys., 78 (2002), pp. 246-252
16. J.-D. Lin, J.-G. Duh, C.-L. Lo, **Mechanical properties and resistance to hydrothermal aging of ceria-and yttria-doped tetragonal zirconia ceramics,** Mater. Chem. Phys., 77 (2002), pp. 808-818
17. S. Lawson, **Environmental degradation of zirconia ceramics,** J. Eur. Ceram. Soc., 15 (1995), pp. 485-502
18. J. Chevalier, B. Cales, J.M. Drouin, **Low-temperature aging of Y-TZP ceramics,** J. Am. Ceram. Soc., 82 (1999), pp. 2150-2154
19. J.F. Bartolomé, I. Montero, M. Díaz, S. López-Esteban, J.S. Moya, S. Deville, L. Gremillard, J. Chevalier, G. Fantozzi, **Accelerated aging in 3-mol%-Yttria-Stabilized tetragonal zirconia ceramics sintered in reducing conditions,** J. Am. Ceram. Soc., 87 (2004), pp. 2282-2285

20. J. Chevalier, L. Gremillard, A.V. Virkar, D.R. Clarke, **The tetragonal-monoclinic transformation in zirconia: lessons learned and future trends,** J. Am. Ceram. Soc., 92 (2009), pp. 1901-1920
21. M. Backhaus-Ricoult, **Interface chemistry in LSM-YSZ composite SOFC cathodes,** Solid State Ion. 177 (2006), pp. 2195-2200
22. R. Kubrin, G. Blugan, J. Kuebler, **Influence of cerium doping on mechanical properties of tetragonal scandium-stabilized zirconia,** J. Eur. Ceram. Soc., 37 (2017), pp. 1651-1656
23. Masini, T. Strohbach, F. Šiška, Z. Chlup, I. Dlouhý, **Electrolyte-supported fuel cell: Co-sintering effects of layer deposition on biaxial strength,** Materials (Basel), 12 (2019)
24. S. Celik, B. Timurkutluk, S. Toros, C. Timurkutluk, **Mechanical and electrochemical behavior of novel electrolytes based on partially stabilized zirconia for solid oxide fuel cells,** Ceram. Int., 41 (2015), pp. 8785-8790
25. I. Denry, J.R. Kelly, **State of the art of zirconia for dental applications,** Dent. Mater., 24 (2008), pp. 299-307
26. L. Gremillard, J. Chevalier, L. Martin, T. Douillard, S. Begand, K. Hans, T. Oberbach, **Sub-surface assessment of hydrothermal ageing in zirconia-containing femoral heads for hip joint applications,** Acta Biomater., 68 (2018), pp. 286-295
27. J. Chevalier, L. Gremillard, **Zirconia as a biomaterial,** Compr. Biomater. II (2017), pp. 122-144
28. P. Khajavi, Y. Xu, H.L. Frandsen, J. Chevalier, L. Gremillard, R. Kiebach, P.V. Hendriksen, **Tetragonal phase stability maps of ceria-yttria co-doped zirconia: from powders to sintered ceramics,** Ceram. Int., 46 (2020), pp. 9396-9405
29. M. Pihlatie, A. Kaiser, P.H. Larsen, M. Mogensen, **Dimensional behaviour of Ni-YSZ anode supports for SOFC under RedOx cycling conditions,** ECS Trans., 7 (2007), pp. 1501-1510
30. S. Ramousse, M. Menon, K. Brodersen, J. Knudsen, U. Rahbek, P.H. Larsen, **Manufacturing of anode-supported SOFC's: processing parameters and their influence,** ECS Trans. S., 7 (2007), pp. 317-327
31. J.-F. Li, R. Watanabe, **Influence of a small amount of Al2O3 addition on the transformation of Y2O3-partially stabilized ZrO2 during annealing,** J. Mater. Sci., 32 (1997), pp. 1149-1153
32. A.A. Nogiwa-Valdez, W.M. Rainforth, P. Zeng, I.M. Ross, **Deceleration of hydrothermal degradation of 3Y-TZP by alumina and lanthana co-doping,** Acta Biomater., 9 (2013), pp. 6226-6235
33. F. Zhang, K. Vanmeensel, M. Inokoshi, M. Batuk, J. Hadermann, B. Van Meerbeek, I. Naert, J. Vleugels, **Critical influence of alumina content on the low temperature degradation of 2-3mol% yttria-stabilized TZP for dental restorations, J**. Eur. Ceram. Soc., 35 (2015), pp. 741-750
34. D.W. Ni, B. Charlas, K. Kwok, T.T. Molla, P.V. Hendriksen, H.L. Frandsen, **Influence of temperature and atmosphere on the strength and elastic modulus of solid oxide fuel cell anode supports,** J. Power Sources, 311 (2016), pp. 1-12
35. H.L. Frandsen, D.J. Curran, S. Rasmussen, P.V. Hendriksen, **High throughput measurement of high temperature strength of ceramics in controlled atmosphere and its use on solid oxide fuel cell anode supports,** J. Power Sources, 258 (2014), pp. 195-203
36. J.B. Wachtman, W.R. Cannon, M.J. Matthewson, **Mechanical Properties of Ceramics** (2nd ed.), John Wiley & Sons (2009)
37. A. Khalili, K. Kromp, **Statistical properties of Weibull estimators,** J. Mater. Sci., 26 (1991), pp. 6741-6752
38. H. Toraya, M. Yoshimura, S. Somiya, **Calibration curve for quantitative analysis of the monoclinic-tetragonal ZrO2 system by X-Ray diffraction,** Commun. Am. Ceram. Soc., 67 (1984), pp. C119-C121
39. H.L. Frandsen, T. Ramos, A. Faes, M. Pihlatie, K. Brodersen, **Optimization of the strength of SOFC anode supports,** J. Eur. Ceram. Soc., 32 (2012), pp. 1041-1052

40. A . Selçuk, A. Atkinson, **Elastic properties of ceramic oxides used in solid oxide fuel cells (SOFC),** J. Eur. Ceram. Soc., 17 (1997), pp. 1523-1532
41. Z.Y. Deng, J.F. Yang, Y. Beppu, M. Ando, T. Ohji, **Effect of agglomeration on mechanical properties of porous zirconia fabricated by partial sintering,** J. Am. Ceram. Soc., 85 (2002), pp. 1961-1965
42. M. Trunec, **Effect of grain size on mechanical properties of 3Y-TZP ceramics,** Ceram. − Silikáty., 52 (2008), pp. 165-171
43. R.E. Fryxell, B.A. Chandler, **Creep, Strength, Expansion, and Elastic Moduli of BeO As a Function of Grain Size, Porosity, and Grain Orientation,** J. Am. Ceram. Soc., 47 (1964), pp. 283-291
44. R.M. Spriggs, **Expression for effect of porosity on elastic Modulus of polycrystalline refractory materials, particularly aluminum oxide,** J. Am. Ceram. Soc., 44 (1961), pp. 628-629
45. D.P.H. Hasselman, **On the porosity dependence of the elastic moduli of polycrystalline refractory materials,** J. Am. Ceram. Soc., 45 (1962), pp. 452-453
46. J.C. Wang, **Young's modulus of porous materials - Part 1 Theoretical derivation of modulus-porosity correlation,** J. Mater. Sci., 19 (1984), pp. 801-808
47. K.K. Phani, S.K. Niyogi, **Young's modulus of porous brittle solids,** J. Mater. Sci., 22 (1987), pp. 257-263
48. D.P.H. Hasselman, R.M. Fulrath, **Effect of small fraction of spherical porosity on elastic moduli of glass,** J. Am. Ceram. Soc., 47 (1964), pp. 52-53
49. J.C. Wang, **Young's modulus of porous materials - Part 2 Young's modulus of porous alumina with changing pore structure,** J. Mater. Sci., 19 (1984), pp. 809-814
50. K.K. Phani, S.K. Niyogi, **Elastic modulus-porosity relationship for Si3N4,** J. Mater. Sci. Lett., 6 (1987), pp. 511-515,
51. A.K. Maitra, K.K. Phani, **Ultrasonic evaluation of elastic parameters of sintered powder compacts,** J. Mater. Sci., 29 (1994), pp. 4415-4419
52. M. Pihlatie, A. Kaiser, M. Mogensen, **Mechanical properties of NiO/Ni-YSZ composites depending on temperature, porosity and redox cycling,** J. Eur. Ceram. Soc., 29 (2009), pp. 1657-1664
53. J. Chevalier, L. Gremillard, S. Deville, **Low-temperature degradation of zirconia and implications for biomedical implants,** Annu. Rev. Mater. Res., 37 (2007), pp. 1-32
54. H. Tsubakino, N. Matsuura, **Relationship between Transformation Temperature and Time–Temperature–Transformation Curves of Tetragonal-to-Monoclinic Martensitic Transformation in Zirconia–Yttria System,** J. Am. Ceram. Soc., 85 (2002), pp. 2102-2106
55. W.Z. Zhu, **Effect of cubic phase on the kinetics of the isothermal tetragonal to monoclinic transformation in ZrO2 (3mol%Y2O3) ceramics,** Ceram. Int., 24 (1998), pp. 35-43
56. P. Timakul, S. Jinawath, P. Aungkavattana, **Fabrication of electrolyte materials for solid oxide fuel cells by tape-casting,** Ceram. Int., 34 (2008), pp. 867-871
57. M. Backhaus-Ricoult, **SOFC - A playground for solid state chemistry,** Solid State Sci., 10 (2008), pp. 670-688
58. Wei, L. Gremillard, **The influence of stresses on ageing kinetics of 3Y- and 4Y- stabilized zirconia,** J. Eur. Ceram. Soc., 38 (2018), pp. 753-760
59. A. Atkinson, **Solid Oxide Fuel Cell Electrolytes-Factors Influencing Lifetime,** in N.P. Brandon, E. Ruiz-Trejo, P. Boldrin (Eds), ***Critical challenges in fuel cells***, Academic Press (2017), pp. 19-35
60. J. Malzbender, W. Fischer, R.W. Steinbrech, **Studies of residual stresses in planar solid oxide fuel cells,** J. Power Sources, 182 (2008), pp. 594-598
61. F.G. Marro, A. Mestra, M. Anglada, **Weibull strength statistics of hydrothermally aged 3 mol% yttria-stabilised tetragonal zirconia,** Ceram. Int., 40 (2014), pp. 12777-12782

62. B.D. Flinn, D.A. Degroot, L.A. Mancl, A.J. Raigrodski, **Accelerated aging characteristics of three yttria-stabilized tetragonal zirconia polycrystalline dental materials,** J. Prosthet. Dent., 108 (2012), pp. 223-230
63. P. Khajavi, J. Chevalier, P. Vang Hendriksen, J.W. Tavacoli, L. Gremillard, H. Lund Frandsen, **Double Torsion testing of thin porous zirconia supports for energy applications: toughness and slow crack growth assessment,** J. Eur. Ceram. Soc., 40 (2020), pp. 3191-3199